Journal of Power Sources 216 (2012) 117–123

Contents lists available at SciVerse ScienceDirect

Journal of Power Sources

journal homepage: www.elsevier.com/locate/jpowsour

Short communication

Nanocomposite SnO_2–Se thin film as anode material for lithium-ion batteries

Xing-Le Ding [a,b], Qian Sun [b], Fang Lu [a], Zheng-Wen Fu [b,*]

[a] Shanghai Key Laboratory of Molecular Catalysts and Innovative Materials, State Key Laboratory of Surface Physics & Department of Physics, Fudan University, Shanghai 200433, China
[b] Department of Chemistry & Laser Chemistry Institute, Fudan University, Shanghai 200433, China

HIGHLIGHTS

- In this paper, nanocomposite SnO_2–Se thin film electrode was fabricated by pulsed laser deposition.
- We examined the electrochemical properties of nanocomposite SnO_2–Se electrode.
- SnO_2–Se/Li cells exhibited a large reversible specific capacity of about 958.8 mAh g^{-1}.
- The reversible oxidation/reduction reaction mechanism of SnO_2–Se with lithium was revealed.

ARTICLE INFO

Article history:
Received 28 February 2012
Received in revised form
10 May 2012
Accepted 10 May 2012
Available online 18 May 2012

Keywords:
Tin oxide–selenide
Pulsed laser deposition
Nanocomposite
Lithium ion batteries

ABSTRACT

The electrochemical properties of nanocomposite SnO_2–Se thin film prepared by pulsed laser deposition method have been investigated by cyclic voltammetry and charge/discharge measurements. A large reversible specific capacity of 958.8 mAh g^{-1} in SnO_2–Se/Li cell cycled between 0.01 and 3.0 V is achieved. Our results have demonstrated that nanocomposite SnO_2–Se exhibits larger capacity and better cycle performance than pure SnO_2 and SnSe. The electrochemical reaction mechanisms of SnO_2–Se with lithium are examined by X-ray diffraction, high resolution transmission electron microscopy, selected-area electron diffraction and spectroelectrochemical measurements. The reversible oxidation/reduction reaction of SnO_2 and selenidation/reduction reaction of SnSe are revealed.

1. Introduction

Tremendous research effort has been devoted to the exploration of novel types of anode materials with larger specific capacities and longer cycle lives instead of the presently used carbonaceous and graphite electrode materials. Tin oxide-based materials as an anode have been attractive in the field of lithium-ion batteries due to a high theoretical capacity of $Li_{4.4}Sn$ (994 mAh g^{-1}) [1]. However, the huge volume change of Li–Sn alloys (above 300% for pure Sn) [2,3] results in the stress-induced pulverization and poor cycling stability of the electrode. Several strategies have been adopted for overcoming these drawbacks of tin oxide-based materials. One of the most common approaches is to employ nanosized materials as recently reviewed [4]. For example, SnO_2 electrodes with various nanostructures have been reported, such as columnar grains [5], spherical particles [6], hollow [7], thin film [8], nanowires [9], nanofibers [10] and macroporous structure [11]. Nanostructures of the electrodes can accommodate volume changes, which can remarkably improve the cyclic performance of the tin oxide-based electrodes [5–11]. On the other hand, Xie et al. have reported that the diffusion coefficients D_{Li} values are 10^{-15}–10^{-13} cm^2 s^{-1} for SnO_2 films by galvanostatic intermittent titration technique (GITT) and suggest that Li-ion diffusion kinetics can be further enhanced by the introduction of other phases into tin oxide thin films [12]. Element doping, such as Zn [13], Sb [14] and F [15], into those nanostructured tin oxides have been confirmed as an effective way. These doped elements could lead to the formation of finer surface morphology and smaller crystallite size, which would provide more reaction sites and facilitate the diffusion of Li, and made it more capable of accommodating the volume changes in cycling. Besides, more researches have been focused on synthesis of various tin-based oxides composites to achieve superior electrochemical behaviors. Fan et al. reported ordered nanostructured tin oxides/carbon composites exhibits a better cyclic performance than pure nano-SnO_2 electrode [16]. SnO_2–CuO nanocomposite studied by Ma et al. showed a reversible capacity of 752 mAh g^{-1} and better

* Corresponding author. Tel.: +86 21 65642522; fax: +86 21 65102777.
E-mail address: zwfu@fudan.edu.cn (Z.-W. Fu).

0378-7753/$ – see front matter © 2012 Elsevier B.V. All rights reserved.
doi:10.1016/j.jpowsour.2012.05.022

cycleability compared with nano-SnO_2 [17]. SnO_2–MnO film delivered by Zhu et al. had 1188.3 mAh g^{-1} of initial discharge capacity and very good capacity retention of 656.2 mAh g^{-1} up to the 30th cycle [18]. Meduri et al. found hybrid tin oxide nanowires containing of Sn, SnO and SnO_2 exhibit a reversible storage capacity greater than 800 mAh g^{-1} over 100 cycles [19]. All these results indicate the diversification of the composites in tin oxide electrode can be beneficial to its electrochemical property.

In our previous work, Fe_2O_3–Se [20] and ZnO–Se [21] nanocomposites showed larger reversible specific capacities and better cyclic stabilities than pure Fe_2O_3 and ZnO, respectively. After discharge, the products were revealed to be Fe or ZnLi, Li_2O and Li_2Se. After charge, metal oxides and selenides were produced. Apparently, these systems with two anions have its unique advantage and the reaction mechanisms with lithium are rather complicated and interesting. In this paper, we will report a novel thin film electrode based on the mixture of SnO_2 and Se as well as its electrochemical properties and reaction mechanisms for the first time. Nanocomposite SnO_2–Se thin films were fabricated by pulsed laser deposition (PLD) method. The electrochemical behavior and physical properties of nanocomposite SnO_2–Se thin film were characterized by galvanostatic cycling, cyclic voltammetry, *in situ* UV–Vis absorption spectra, high resolution transmission electron microscopy (HRTEM) and selected-area electron diffraction (SAED). The motivation of this study is to explore the influence of inducing Se into SnO_2 thin film as an anode material for lithium-ion batteries and to elucidate the electrochemical reaction mechanism of nanocomposite electrode with lithium.

2. Experimental

A PLD system for the fabrication of thin films in a vacuum chamber was described previously [22]. Experimental conditions for depositing thin films are described as follows: A 355 nm laser beam from a Q-switched Nd: yttrium aluminum garnet laser (Spectra Physics GCR-150) with a pulsed repetition rate of 10 Hz and a pulsed width of 5 ns was focused onto the surface of the target. The incident angle between the laser beam and the target surface normal was 45°. The laser intensity was about 2 J cm^{-2}. The distance between the target and the substrate was 4 cm. The sputtering chamber was evacuated below 10^{-3} Pa during deposition. Composite target consisting of SnO_2 and Se were obtained by cold pressing SnO_2 powder (99.95%, Alfa Aesar) and Se powder with a molar ratio of 1:0.8. The films were deposited on a stainless steel substrate at room temperature. The thickness of the as-deposited films is about 80 nm for the depositing time of 30 min. Weight of thin film was directly obtained by subtracting the original substrate weight from total weight of substrate and deposited thin film onto its surface, which were examined by electrobalance (BP 211D, Sartorius), and was about 0.05 mg with the area of 1.0 cm^2.

X-ray diffraction (XRD) patterns and the morphology of the SnO_2–Se thin film electrodes were recorded by a Rigata/max-C diffractometer with Cu Kα radiation (λ = 1.5406 Å) and scanning electron microscopy (SEM) (Cambridge S-360), respectively. HRTEM and SAED measurements were carried out by a JEOL 2010 TEM at 160 kV accelerating voltage. An energy-dispersive X-ray analysis (EDX, Kevex EDX spectrometer) coupled with the microscope was used to determine the chemical composition of the products. *In situ* spectroelectrochemical measurements were further utilized to obtain the *in situ* UV–Vis absorption spectra of the deposited thin film through the electrochemical reaction, where SnO_2–Se thin film was deposited on Au coated quartz plate and used as a working electrode. Details for the *in situ* spectroelectrochemical measurements have been described elsewhere [23].

For the electrochemical measurements, the cells were constructed by using the as-deposited SnO_2–Se thin film as a working electrode and two lithium sheets as a counter electrode and a reference electrode, respectively. The electrolyte consisted of 1 M $LiPF_6$ in a nonaqueous solution of ethylene carbonate (EC) and dimethyl carbonate (DMC) with a volume ratio of 1:1 (Merck). Charge–discharge measurements were performed at room temperature with a Land BT 1–40 battery test system. The cells were cycled between 0.01 V and 3.0 V vs. Li/Li^+ at a current density of 15 μA cm^{-2}.

To avoid the exposure to air or water, the model cells at different stages including the as-deposited, discharged to 0.01 V and recharged to 3.0 V were dismantled in an Ar-filled glove box and the electrodes were rinsed in anhydrous DMC to eliminate residual salts.

3. Results and discussion

Pulsed laser deposition method is generally considered to be effective in fabricating thin film with high deposition rate, easy control over film thickness, and original bulk target transferring. However, PLD process is rather complicated if a mixed target is ablated. In order to identify the composition and structure of the as-deposited thin films, XRD, TEM and SAED measurements were carried out and the results are shown in Fig. 1. Fig. 1(a) shows XRD pattern of the as-deposited thin films. Three diffraction peaks appearing at 2θ = 26.6, 33.9, and 51.9° can be assigned to (110), (101), and (211) reflection of SnO_2 (JCPDS 77-0451). However, no any peak from Se is observed. This may be due to the size of its particles smaller than the X-ray coherence length and thus cannot be detected by XRD technology. On the other hand, crystalline lattices can be clearly observed in the high resolution TEM image of SnO_2–Se thin film (Fig. 1(b)). They can be indexed to (110) plane of SnO_2. SAED pattern in this region shown in Fig. 1(c) exhibits some clear concentric rings and some spots. All d-spacings corresponding to these rings and spots derived from the SAED spectra are listed in Table 1 and could be assigned to SnO_2 ($P4_2/mnm$) and Se ($P3_121$). These results indicate that the as-deposited film mainly consists of SnO_2 and Se. According to EDX spectra (not shown here), the mole ratio of Sn and Se is estimated to be about 2.65: 1.00. The inconsistent stoichiometry between the thin film and the original target implies the loss of Se during the laser ablation.

The galvanostatic cycling curves of nanocomposite SnO_2–Se/Li cells at room temperature is shown in Fig. 2(a). It was cycled between 0.01 and 3.0 V at a current density of 15 μA cm^{-2}. The open-circuit voltage of the cell lies at 1.9 V. There are three sloping discharge plateaus appearing at 1.54, 0.91 and 0.33 V. The initial discharge capacity of 1188.6 mAh g^{-1} is obtained, corresponding to about 6.5 Li per 0.726 SnO_2:0.274 Se unit (referred as SnO_2–Se unit in the following text), which is close to its theoretical capacity of 1267.4 mAh g^{-1}. The plateau at 0.91 V vanished in the second discharge, indicting an irreversible electrochemical reaction while the plateau at 1.54 V was slightly declined to 1.46 V. The subsequent charging curves are identical to that in the first cycle. The second discharge process of the cell yields a reversible discharge capacity of about 959 mAh g^{-1}, corresponding to 5.2 Li per SnO_2–Se unit. After the 100th cycles, a reversible capacity of 773.7 mAh g^{-1} could be obtained, indicating excellent capacity retention of the thin film electrode with the loss of capacity less than 0.19% per cycle. Cycling performance and coulombic efficiency of SnO_2–Se thin film electrodes as a function of the cycle number are presented in Fig. 2(b). The discharge capacities of pristine SnSe thin film from literature [24] and SnO_2 thin film from our own work are also included for comparison. In the initial 120th cycles, the coulombic efficiency can be excellently kept over 96%. Besides, the specific capacity of

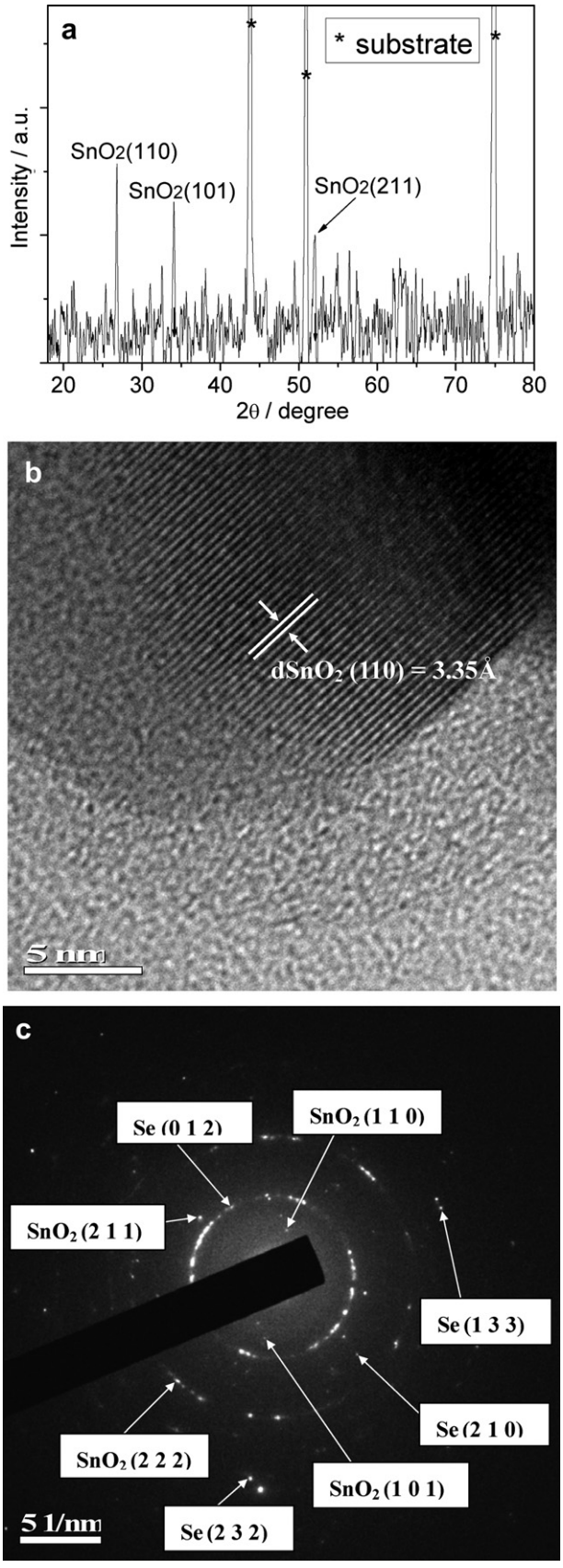

Fig. 1. (a) X-ray diffraction pattern, (b) High resolution TEM images and (c) the SAED spectrum of the as-deposited SnO_2–Se thin film electrodes.

Table 1
d-Spacings (Å) derived from SAED analysis of the as-deposited and the first discharging to 0.01 V and recharging to 3.0 V of SnO_2–Se thin film electrode. JCPDS standards for SnO_2, Se, $Li_{22}Sn_5$, Li_2O, Li_2Se, SnSe are shown for reference.

As-deposited			
Our result	$SnO_2(P4_2/mnm)$	Our result	$Se(P3_121)$
3.34	3.36 (110)	2.05	2.07 (012)
2.64	2.65 (101)	1.42	1.43 (210)
1.76	1.77 (211)	0.89	0.89 (133)
1.16	1.16 (222)	0.81	0.82 (232)
$a = 4.73 \pm 0.01$	$a = 4.75$	$a = 4.34 \pm 0.02$	$a = 4.36$
$c = 3.18 \pm 0.02$	$c = 3.20$	$c = 6.94 \pm 0.03$	$c = 4.96$

First discharging to 0.01 V					
Our result	$Li_{22}Sn_5(F23)$	Our result	$Li_2Se(Fm\bar{3}m)$	Our result	$Li_2O(Fm\bar{3}m)$
1.99	1.98 (771)	1.83	1.81 (311)	2.68	2.67 (111)
1.26	1.26 (1533)	1.38	1.38 (331)	1.14	1.15 (400)
$a = 19.7 \pm 0.1$	$a = 19.8$	$a = 6.03 \pm 0.02$	$a = 6.01$	$a = 4.59 \pm 0.02$	$a = 4.62$

First charging to 3.0 V			
Our result	$SnO_2(Fm\bar{3}m)$	Our result	$SnSe(Fm\bar{3}m)$
2.86	2.84 (111)	2.10	2.12 (220)
1.47	1.48 (311)	1.82	1.81 (311)
1.09	1.10 (420)	1.72	1.73 (222)
		1.33	1.34 (420)
$a = 4.91 \pm 0.03$	$a = 4.93$	$a = 5.97 \pm 0.02$	$a = 5.99$

SnO_2–Se thin-film electrode exhibited much better stability than that of other two and only 19% of the reversible discharge capacity was declined after 100 cycles. Apparently, the addition of Se can highly improve the electrochemical behavior of SnO_2.

In order to highlight the electrochemical performance of the present material, a comparison of SnO_2–Se thin film cathode prepared in this study with those of previous works has been operated. The results are summarized in Table 2. Due to the addition of pure Se, the reversible capacity of SnO_2–Se thin film prepared by PLD can be quite high with a relatively large initial capacity of 1188.6 mAh g^{-1}. Moreover, the cyclability of this thin film material is also extremely outstanding, which indicates that a prominent improvement of the electrochemical behavior has been reached by synthesis of the SnO_2–Se nanocomposited thin film.

Fig. 2(c) presents the first three cyclic voltammograms for the as-deposited nanocomposite SnO_2–Se between 0.01 and 3.0 V measured at a scan rate of 0.2 mV s^{-1}. Four cathodic current peaks at 1.46, 1.33, 0.91 and 0.25 V are observed in the initial reduction process. The peak at 0.91 V disappeared in the subsequent cycles. There are three anodic peaks at about 1.77, 0.98 and 0.48 V in the initial charging process, all of which have a good repetitiveness in the subsequent cycles, indicating that the reactions were highly reversible. The couple of reduction and oxidation peaks at about 0.25 V during the discharge and at 0.48 V during the charge cycles should mainly result from the alloy reaction of Sn with Li [2,27,28]. The cathodic peak at 0.9 V disappeared in subsequent cycles could possibly be attributed to the irreversible reaction of SnO_2 [6] as well as solid state electrolyte interface (SEI) film [21]. In the second cycle, a new peak at 0.55 V emerged in the discharging process. This peak remains well in the third cycle, indicating a new electrochemical reaction.

Fig. 3(a), (b) and (c) shows the morphology of the as-deposited, discharged and charged SnO_2–Se thin films, respectively. It can be seen that the as-deposited thin film is a flat film consisting of nanosized SnO_2–Se particles. After discharging to 0.01 V, the surface morphology is mostly changed and becomes quite different from the initial film (Fig. 3(b)), whereas the components are the same as the as-deposited film according to EDX spectra. Apparently,

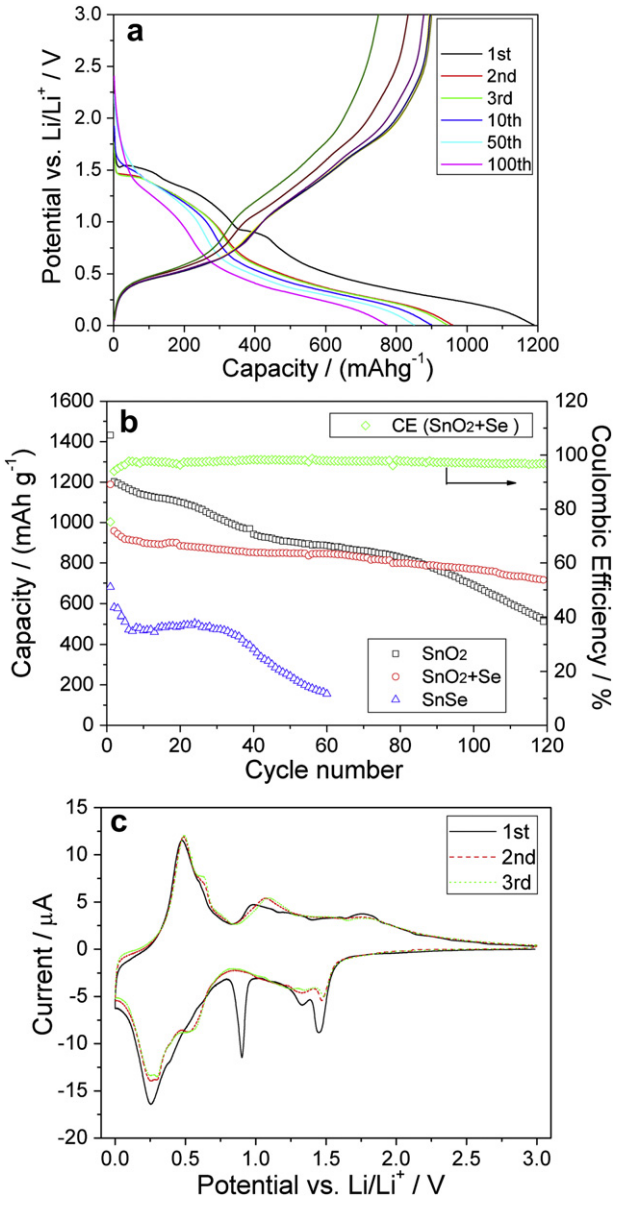

Fig. 2. (a) Galvanostatic cycling curves in a voltage range of 0.01–3.0 V for the as-deposited SnO_2–Se thin film at a current density of 15 μA cm^{-2}; (b) Coulombic efficiency of SnO_2–Se thin film and Cycling performance of SnO_2–Se thin film, SnO_2 thin film, SnSe thin film as a function of cycle number; (c) The first three cyclic voltammograms of the as-deposited SnO_2–Se thin film.

the surface becomes rough and the particles aggregate together to form large grains. It should be attributed to the electrochemical decomposition of SnO_2–Se and volume expansion during the formation of SnLi alloy. The grains on the surface are most likely due to the agglomeration of nano-size particles and electrolyte interface surrounding the agglomerates. After recharging to 3.0 V (Fig. 3(c)), the large grains are decomposed and shrinking. The size of the grains is obviously reduced. The remarkable morphology changes during discharge and charge imply the huge phase transformation and volume change of the thin film in lithiation/delithiation process.

In order to gain insight into the reaction mechanism of SnO_2–Se thin film with lithium, *ex situ* TEM and SAED measurements were employed to detect the composition and structure of the lithiated and delithiated thin films. Fig. 4(a) shows the typical TEM image of

Table 2
Electrochemical properties of various tin-based materials as negative electrodes produced by this work and from literatures.

Sample	Initial discharge capacity (mAh g^{-1})	Initial capacity loss (mAh g^{-1})	Discharge capacity at 30th cycle (mAh g^{-1})	Voltage range (V)	Reference
Nanostructure:					
SnO_2 porous spheres	601	11	468	0.05–1.35	[6]
SnO_2 hollow spheres	1140	25	630	0.01–2.5	[7]
SnO_2 thin film	1426	324	910	0.01–3.0	[8]
SnO_2 nanowires	2130	1210	310	0.05–1.5	[9]
SnO_2 nanofibers	1650	820	560	0.05–1.5	[10]
M-Doped SnO_2:					
Zn-doped SnO_2	515[a]	70[a]	180[a]	0.0–1.7	[13]
Sb-doped SnO_2 (9:1)	2170	620	700	0.005–2.0	[14]
Sb-doped SnO_2 (5:1)	1990	740	510	0.005–2.0	[14]
Composite:					
SnO_2-Se thin film	1189	230	867	0.01–3.0	This work
Macroporous SnO_2/C	1705	800	700	0.05–1.5	[11]
SnO_2–CuO	1585	833	730	0.0–1.0	[17]
SnO_2–MnO	1188	513	656	0.01–3.0	[18]
RG-O/SnO_2	2140	1035	649	0.01–2.0	[25]
$SnB_{0.6}P_{0.4}O_{2.9}$	495	120	175	0.0–1.5	[26]

[a] μAh cm^{-2} μm^{-1}.

the lithiated SnO_2–Se thin film. SAED pattern in this region (Fig. 4(b)) exhibits some rings made up of discrete spots and some bright particles, which can be indexed to $Li_{22}Sn_5$, Li_2Se and Li_2O according to Table 1. The result confirms the decomposition of SnO_2–Se and the formation of $Li_{22}Sn_5$, Li_2Se and Li_2O after discharging to 0.01 V. HRTEM image after the thin film recharging to 3.0 V is shown in Fig. 5(a). The crystal lattices clearly observed can be attributed to (111) plane of SnO_2. The corresponding SAED pattern (Fig. 5(b)) exhibits some clear concentric rings, indicating nanosized polycrystalline nature of the delithiated thin film. After calculation, all d-spacings derived from the SAED can be indexed to SnO_2 and SnSe (Table 1). The spacing group of SnO_2 after charged is $Fm\bar{3}m$, which is different from that of the deposited thin film.

As we considered that the structure would change and the formation of new products in the electrochemical reaction of SnO_2–Se thin film electrode might cause different optical absorption characteristics over the visible region, it should be believed that the *in situ* UV–Vis absorption spectra based on as-deposited SnO_2–Se thin film could provide some information on the lithiation reaction. Fig. 6(a) and (b) shows *in situ* UV–Vis absorption spectra collected at various states (*x* values) of the initial discharge and charge cycle of SnO_2–Se/Li cell at room temperature, respectively. SnO_2–Se thin film electrode was deposited on Au coated quartz substrate at room temperature. During the initial discharge and charge processes, the thin-film electrodes show strong absorption from 500 nm to 900 nm. The shapes of absorption spectra are alike during the discharging and charging processes of SnO_2–Se/Li cell, without any shift of the absorption peaks when Li number increases and decreases. In addition, a progressive increase and decrease of the *in situ* UV–Vis absorption spectra intensity are observed when the Li ions are reduced to 0.01 V and further oxidized to 3.0 V in the discharge and charge cycle, respectively. In order to compare the absorbance change of the discharge and charge processes, the absorbance at 698 nm as a function of *x* value are presented in Fig. 6(c). It can be seen that the absorbance changes exhibit an irreversible feature in initial discharging and charging processes and a reversible reaction in second cycle, which is similar to its electrochemical behavior mentioned above. At the *x* value more than about 3.5, the amplitudes of all *in situ* absorbance spectra dramatically increases/decreases during discharging/charging, which should be caused by alloy/dealloy reaction of Sn

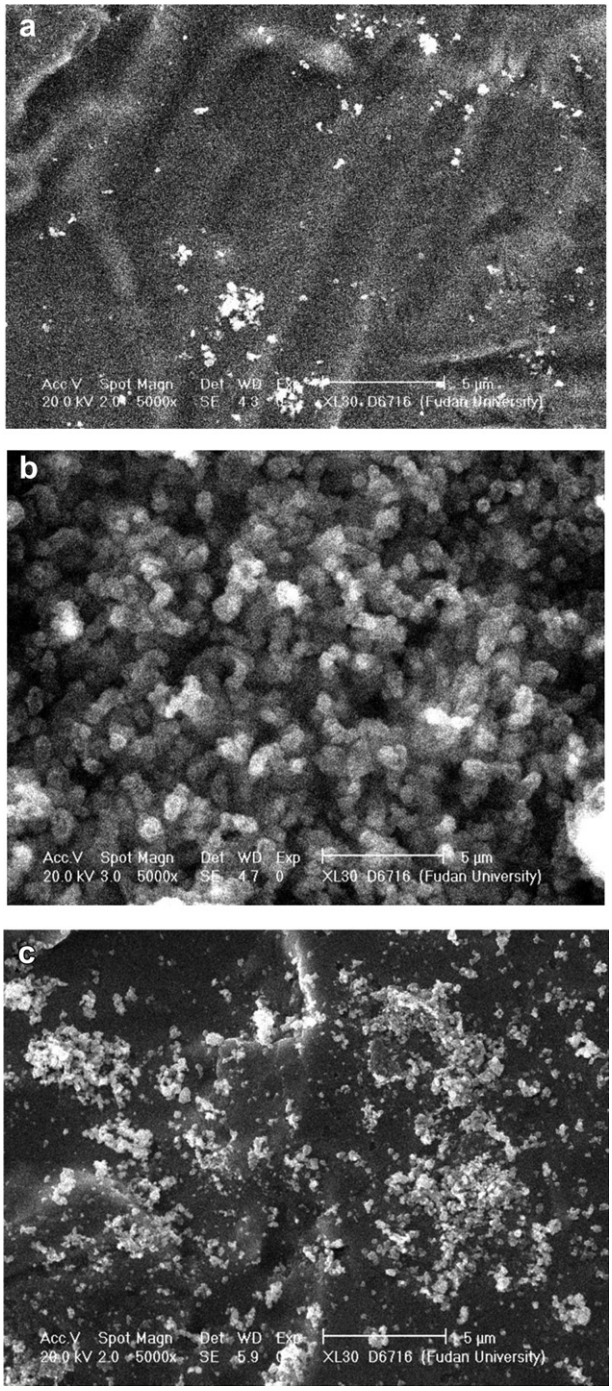

Fig. 3. SEM images of the SnO_2–Se thin film for (a) the as-deposited; (b) after the discharging to 0.01 V and (c) after the recharging to 3.0 V.

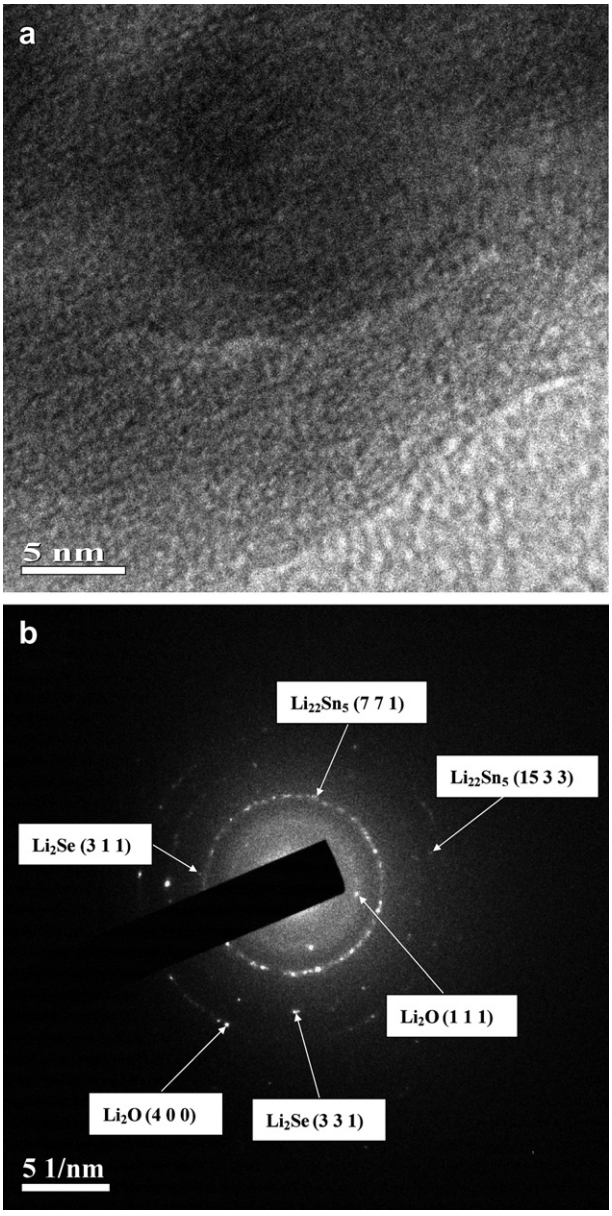

Fig. 4. (a) *Ex situ* high resolution TEM images and (b) SAED spectrum of SnO_2–Se thin film electrodes after the discharging to 0.01 V.

with Li. Besides, the differences of absorbance spectra between the first and second discharging processes provide an evidence that the charged product is not the same as the original.

Based on the above data, the electrochemical reaction mechanism of SnO_2–Se with lithium involving the following steps is proposed.

Initial discharging process:

$$SnO_2 + 4Li^+ + 4e^- \rightarrow Sn + 2Li_2O \quad (1)$$

$$Se + 2Li^+ + 2e^- \rightarrow Li_2Se \quad (2)$$

$$Sn + 4.4Li^+ + 4.4e^- \rightarrow Li_{4.4}Sn \quad (3)$$

Subsequent cycles:

$$Li_{4.4}Sn \leftrightarrow Sn + 4.4Li^+ + 4.4e^- \quad (4)$$

$$Sn + Li_2Se - 2e^- \leftrightarrow SnSe + 2Li^+ \quad (5)$$

$$Sn + 2Li_2O - 4e^- \leftrightarrow SnO_2 + 4Li^+ \quad (6)$$

These steps during the discharge and charge processes agree with CV curves, as shown in Fig. 2(c). In the initial discharge, the peak at 0.91 V is caused by solid state electrolyte interface (SEI) film. Cathodic peaks at 1.46 and 1.33 V in the second cycle could be attributed to the decomposition reaction of SnO_2 (Reaction (1)). The wide cathodic peaks at 0.40 V and 0.25 V corresponds to the lithium

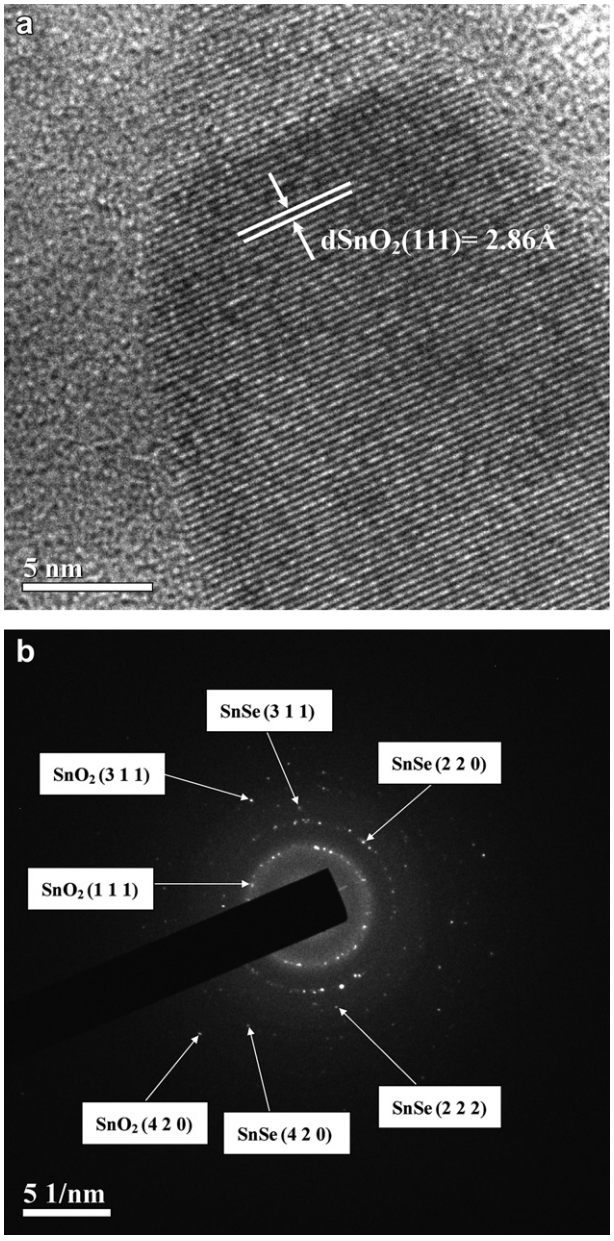

Fig. 5. (a) *Ex situ* high resolution TEM images and (b) SAED spectrum of SnO_2–Se thin film electrodes after the charging to 3.0 V.

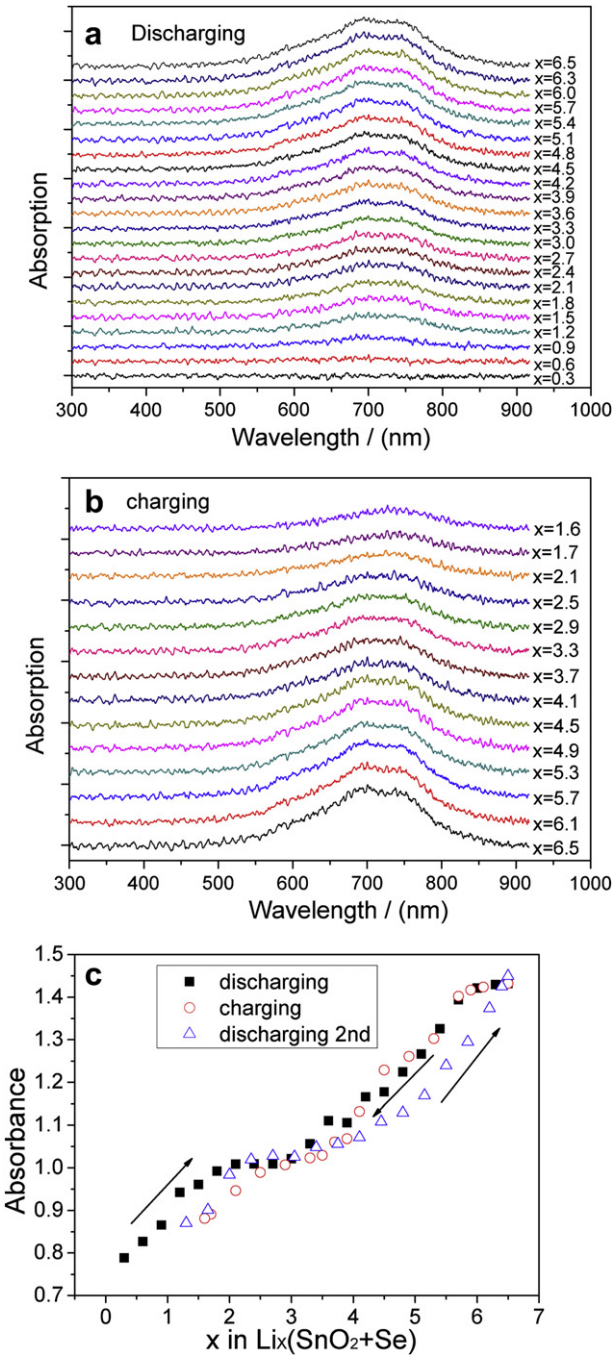

Fig. 6. Selected *in situ* UV–Vis absorption spectra obtained (a) during first discharging of SnO_2–Se to 0.01 V and (b) during charging of SnO_2–Se to 3.0 V; (c) Absorbance at 698 nm as a function of *x* value of reacted Li.

alloying reaction of Se and Sn (reactions (2) and (3)). The cathodic peaks from these decomposition reactions of SnO_2 and SnSe seem almost overlapped in the subsequent cycles. In the charging process, the peak at 0.48 V is the dealloying reaction of $Li_{4.4}Sn$ (reaction (4)). The anodic peaks at about 0.98 and 1.77 could be attributed to the formation of SnO_2 and SnSe.

Reactions (1)–(3) occur in the first discharge process with the structure transformation of the initial polycrystalline SnO_2 and Se. In reaction (1), SnO_2 and Li produce nanosized Sn and Li_2O. In reactions (2) and (3), Se and Sn could alloy with lithium during further discharge. The subsequent cycling processes involved reactions (4)–(6) are completely reversible. It can explain the repeatability of CV curves. These reactions includes alloy/dealloy reactions of Sn with Li, the oxidation/reduction reaction between Sn and SnO_2 and the selenidation/reduction reaction between Sn and SnSe. In reactions (5) and (6), it is convinced that Sn has fully reacted with Li_2O and Li_2Se based on the high reversible capacity and the characterization of SAED. It is estimated that about 27.4% Li_2O/Li_2Se doesn't participate in the electrochemical reaction with metal Sn. This should be responsible for the irreversible capacity in the initial cycle. But the residual Li_2O/Li_2Se could buffer the volume change and release the inner stress during phase transition in subsequent cycles, which leads to the prominent capacity retention. It is believed that the electrochemical performance of nanocomposite SnO_2–Se thin film can be improved further after

optimizing the molar ratio of SnO_2 to Se. The fact that only 19.3% of the reversible discharge capacity was declined during the initial 100th cycles have demonstrated that it is a very effective way to add Se into SnO_2 for the purpose of improving cycle performance. If comparing with the data reported previously, nanosized SnO_2 always has a large capacity loss upon repeated cycling. For example, Fan et al. [16] showed that only 42.8% of the capacity was reserved for an ONTC electrode over 30th cycles. The capacity of the SnO_2–MnO composite [18] fade from an initial capacity of 1188 mAh g^{-1} to 656 mAh g^{-1} after 30th cycles. In the charging process, not all Sn can react with Li_2O and come back to SnO_2. It is a partly reversible process with the gradual formation of inactive Li_2O during the cycles. This will result in a large capacity loss of nanosized tin oxide-based materials. Apparently, nanocomposite SnO_2–Se thin film as an anode exhibits the superior cycle performance. In the present case, nanosized metal tin could drive the decomposition of Li_2Se instead of the "dead" inactive Li_2O to hold the high reversible capacity. Meantime, the inactive Li_2O could be considered as the matrix-glue holding small tin particles to cushion the volume change of the Li–Sn alloys for the cyclability improvement. This kind of electrochemical reaction mechanism of SnO_2–Se with lithium may reopen new opportunities in this fascinating field of storing Li for Li-ion batteries.

4. Conclusions

Nanocomposite SnO_2–Se thin film has been fabricated by pulsed laser deposition for the first time. The addition of Se into SnO_2 has lead to a higher reversible capacity and better cycle performance compared to pure SnO_2 and SnSe. Galvanostatic cycling showed a large reversible capacity around 958.8 mAh g^{-1}. The electrochemical reaction mechanisms of SnO_2–Se with lithium can be concluded as following: after the discharge process, $Li_{4.4}Sn$, Li_2O and Li_2Se were produced. After the recharge process, SnO_2 and SnSe were formed. Subsequent cycles involve the reversible oxidation/reduction reaction of SnO_2 and selenidation/reduction reaction of SnSe. Residual Li_2O/Li_2Se after initial discharge may play an important role in the improvement of its cyclic performance. High reversible capacity and good stable cycle make nanocomposite SnO_2–Se a promising anode for high energy density Li-air cells.

Acknowledgements

This work was financially supported by 973 Program (No. 2011CB933300) of China, and Science & Technology Commission of Shanghai Municipality (08DZ2270500 and 11JC1400500).

References

[1] Y. Idota, T. Kubota, A. Matsufuji, Y. Maekawa, T. Miyasaka, Science 276 (1997) 1395–1397.
[2] I.A. Coutney, J.R. Dahn, J. Electrochem. Soc. 144 (1997) 2045–2052.
[3] T. Brousse, R. Retoux, U. Herterich, D.M. Schleich, J. Electrochem. Soc. 145 (1998) 1–4.
[4] D. Deng, M.G. Kim, J.Y. Lee, J. Cho, Energy Environ. Sci. 2 (2009) 818–837.
[5] Y.L. Zhang, Y. Liu, M.L. Liu, Chem. Mater. 18 (2006) 4643–4646.
[6] L. Yuan, Z.P. Guo, K. Konstantinov, H.K. Liu, S.X. Dou, J. Power Sources 159 (2006) 345–348.
[7] X.W. Lou, Y. Wang, C.L. Yuan, J.Y. Lee, L.A. Archer, Adv. Mater. 18 (2006) 2325–2329.
[8] M.Z. Xue, Z.W. Fu, Electrochem. Solid State Lett. 9 (2006) A468–A470.
[9] M.S. Park, G.X. Wang, Y.M. Kang, D. Wexler, S.X. Dou, H.K. Liu, Angew. Chem. Int. Ed. 46 (2007) 750–753.
[10] Z.X. Yang, G.D. Du, C.Q. Feng, S. Li, Z.X. Chen, P. Zhang, Z.P. Guo, X.B. Yu, G.N. Chen, S.Z. Huang, H.K. Liu, Electrochim. Acta 55 (2010) 5485–5491.
[11] C.H. Yim, E.A. Baranova, F.M. Courtel, Y. Abu-Lebdeh, I.J. Davidson, J. Power Sources 196 (2011) 9731–9736.
[12] J. Xie, N. Imanishi, A. Hirano, Y. Takeda, O. Yamamoto, X.B. Zhao, G.S. Cao, Solid State Ionics 181 (2010) 1611–1615.
[13] M. Torabi, S.K. Sadrnezhaad, J. Power Sources 196 (2011) 399–404.
[14] F.D. Wu, M.H. Wu, Y. Wang, Electrochem. Commun. 13 (2011) 433–436.
[15] C.W. Kwon, G. Campet, J. Portier, A. Poquet, L. Fournes, C. Labrugere, B. Jousseaume, T. Toupance, J.H. Choy, M.A. Subramanian, Int. J. Inorg. Mater. 3 (2001) 211–214.
[16] J. Fan, T. Wang, C.Z. Yu, B. Tu, Z.Y. Jiang, D.Y. Zhao, Adv. Mater. 16 (2004) 1432–1436.
[17] M.Y. Ma, Z.Q. He, Z.B. Xiao, K.L. Huang, L.Z. Xiong, X.M. Wu, Trans. Nonferrous Met. Soc. China 16 (2006) 791–794.
[18] X.J. Zhu, Z.P. Guo, P. Zhang, G.D. Du, C.K. Poh, Z.X. Chen, S. Li, H.K. Liu, Electrochim. Acta 55 (2010) 4982–4986.
[19] P. Meduri, C. Pendyala, V. Kumar, G.U. Sumanasekera, M.K. Sunkara, Nano Lett. 9 (2009) 612–616.
[20] W.J. Li, Y.N. Zhou, Z.W. Fu, Electrochim. Acta 55 (2010) 8680–8685.
[21] Y.N. Zhou, W.J. Li, Z.W. Fu, Electrochim. Acta 59 (2012) 435–440.
[22] Q.Z. Qin, Z.W. Fu, Adv. Mater. 109 (1999) 1119–1123.
[23] Z.W. Fu, F. Huang, Y. Zhang, Y. Chu, Q.Z. Qin, J. Electrochem. Soc. 150 (2003) A714–A720.
[24] M.Z. Xue, J. Yao, S.C. Cheng, Z.W. Fu, J. Electrochem. Soc. 153 (2006) A270–A274.
[25] X.J. Zhu, Y.W. Zhu, S. Murali, M.D. Stoller, R.S. Ruoff, J. Power Sources 196 (2011) 6473–6477.
[26] S. Machill, T. Shodai, Y. Sakurai, J. Yamaki, J. Power Sources 73 (1998) 216–223.
[27] N.C. Li, C.R. Martin, J. Electrochem. Soc. 148 (2001) A164–A170.
[28] M.S. Park, G.X. Wang, Y.M. Kang, D. Wexler, S.X. Dou, H.K. Liu, Angew. Chem. Int. Ed. 119 (2007) 764–767.